Validation of Computational Fluid Dynamics Simulations for Realistic Flows

Dr. Farhad Davoudzadeh
Air Force Research Laboratory
4 Draco Drive, Building 8351
Edwards AFB, CA 93524-7680
USA

Farhad.Davoudzadeh@us.af.mil

ABSTRACT

Strategies used to verify and validate computational fluid dynamics (CFD) calculations are described via case studies of realistic flow simulations, each representing a complex flow physics and complex geometry. Critical areas of importance to validation of a calculation are pointed out through various high fidelity physics- and engineering-based simulations. These areas include the physical model, conceptual model, boundary conditions, initial conditions, geometry, grid density and distribution, turbulence model, and numerical dissipation. Appropriate selection and exercise of the above items depend upon thorough understanding of the physics of the problem and require considerable experience on addressing them utilizing CFD codes. The cases presented include the most frequently encountered flow features of separation, swirl and rotation as observed in engineering applications such as aircraft gas combustors and turbomachinery. Each simulation considers the salient physical features involved and resolves them to the level required by the purposes for which they are being used. In many of the simulations presented, unstructured grids and parallel computing are used to minimize the overall time needed to achieve a numerical solution. In these cases, the numerical scheme incorporated allows use of a large number (thousands) of processors in parallel, to shorten the solution time and to provide speed-ups that do not deteriorate with the addition of more processors. Verification studies compare the exact analytical solutions with those obtained using various numerical schemes. In these studies preservation of a vortex convecting through a calculation domain is used to assess the numerical accuracy of time-dependent numerical schemes. Magnitude and distribution changes of field variables, primarily pressure, are quantified to obtain accurate assessment of numerical errors with first-order time-accurate central-difference, second-order time-accurate iterative implicit, and fifth-order accurate upwind-biased schemes. A scheme which minimizes numerical error involves preservation of both the vortex strength and the vortex structure.

1.0 INTRODUCTION

A considerable amount of work has gone into developing metrics for validation and verification of the computational codes that are developed and used for modelling and simulation of fluid flow [1-12]. American Institute of Aeronautics and Astronautics (AIAA), and American Society of Mechanical Engineers (ASME) have declared policy statements and guidelines for the verification and validation of computational fluid dynamics simulations [13-16]. These metrics and guidelines cover issues such as assessment for the iterative convergence, spatial grid convergence, temporal convergence, comparison of the CFD results to experimental

Davoudzadeh, F. (2007) Validation of Computational Fluid Dynamics Simulations for Realistic Flows. In *Computational Uncertainty in Military Vehicle Design* (pp. 24-1 – 24-16). Meeting Proceedings RTO-MP-AVT-147, Paper 24. Neuilly-sur-Seine, France: RTO. Available from: http://www.rto.nato.int.

data, uncertainty analysis, and assessment of the computer programs or codes to check for coding errors, to mention a few. Fulfilling all the above mentioned metrics and following all the guidelines still, does not provide a guarantee that a code is truly verified and validated. As Roche [13] mentioned it may never be appropriate to say that a code itself is validated. The important factor is the experience and the ability of the user in understanding the underlying physics that govern a given flowfield and his subsequent evaluation on whether a code can reliably model that physics. Otherwise, the code needs to be validated for the given problem in hand.

This paper describes a number of numerical simulations for realistic cases where an assessment of the underlying physics of the flow is accompanied with a methodical approach on examining whether the code can simulate those physics or not, prior to applying the code for the eventual simulation.

2.0 VORTEX PRESERVATION TEST

Vortex preservation test can be used to validate the capability of a code for time accurate preservation of the vortical structures in the flow, and the strength of those vortical structures as they are convected by the flow downstream. Vortical structures prevail in a number of realistic flows. The performance of various devices and vehicles are dramatically affected by these vortical structures. It is therefore crucial that the codes used in these applications, where vortical structures play a role, are capable of maintaining these structures. Examples of the flows where preserving vortical structures is essential for meaningful results are flowfields of hurricanes, tornados, blade vortex interaction (BVI), maneuvering submarines, and reacting flows in combustion chambers.

Preservation of a vortex convecting through a computational domain is used here to assess the numerical accuracy of time-dependant Navier-Stokes numerical schemes. Magnitude and distribution changes of field variables, primarily pressure, are quantified to obtain accurate assessment of numerical errors with first-order time-accurate central-difference, second-order time-accurate iterative implicit, and fifth-order accurate upwind-biased schemes. During convection of a Lamb-type vortex [l7] in a freestream, pressure is at minimum in the vortex core and increases concentrically and asymptotically to the freestream value with radial distance from the vortex center. A numerically dissipative scheme cannot maintain this pressure minimum at the vortex center, and core pressure increases as the vortex convects downstream. In inviscid flow calculations such as those solving Euler equations, the pressure distribution should remain unaltered by convection but numerically dissipative schemes result in a predicted pressure which increases with downstream distance caused by the numerically induced vortex decay. The concentric structure of the vortex should also remain unaltered with downstream convection, however certain numerical schemes cannot maintain concentricity of isobars around the vortex, instead patterns are distorted and characterized by solution oscillation waviness. A scheme which minimizes numerical error involves preservation of both level and distribution of, for example the pressure minimum and concentricity of the vortex, respectively. Preservation of concentricity alone may be insufficient and misleading.

A series of calculations using a conventional first-order-accurate, central-difference scheme and a second order unsteady iterative implicit scheme are performed by solving the time dependent Euler/Navier-Stokes equations [18]. Variation of vortex core pressure against number of core radii travelled by the vortex is monitored to measure the time and spatial accuracy of the Navier-Stokes code. These calculations are performed to assess the vortex preservation capabilities of the numerical procedure and to indicate areas where refinement would be required. Based on the results of these calculations, the code is further developed to provide the ability to perform practical studies of airfoil-vortex interaction [19]. Details of the numerical scheme, governing equations and the vortex definition are given in [18].

2.1 COMPUTATIONAL GRID

The computational domain used for the convection of the vortex is shown in Figure 1. The grid is non-uniform, with equal spacing ($\Delta x = \Delta y = 1/8$) used in the central region containing the vortex path and a stretched grid is used to extend the physical domain to the far field. The boundaries of the grid are 245 x 200 radii in length to width, the core radius of the vortex being 1.0. The boundaries of the equally spaced grid region, the overall boundaries and the vortex path are shown in Figure 1. The boundaries of the grid are considerably far from the vortex path to eliminate any boundary effects on the vortex.

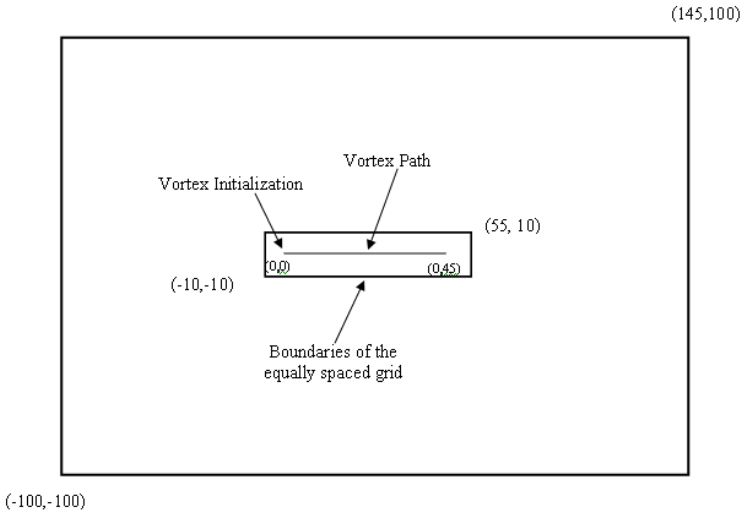

Figure 1: Physical domain and the vortex path

2.2 FIRST ORDER IN TIME, CENTRAL DIFFERENCE SCHEME

A calculation is performed to determine the flow characteristics associated with a Lamb-type vortex convection in a freestream, using the central difference scheme with first order accuracy in time, without any inner iteration at each time step. In these calculations, the reference length is the vortex core radius, the reference flow conditions are the free stream conditions with the Mach number M = 0.536. Time t, is made dimensionless by freestream velocity and the vortex core radius, e.g. an increment, $\Delta t = 1.0$, is the time required for a particle at freestream velocity to travel one vortex core radius. Curve A in Figure 2 shows the variation of the vortex core pressure with the distance travelled for this first-order scheme, second-order iterative implicit, and fifth-order upwind-biased scheme. As shown by the curve A in Figure 2, the predicted core pressure is increased drastically compared to its initial value. It is evident that the first-order time accurate scheme is very dissipative; an improvement is needed for vortex preservation. This is achieved by using the second-order unsteady iterative implicit scheme described in the next section. However, the results of this calculation are consistent with those obtained by Rai [20] who used the first-order time accurate Beam and Warming scheme. It should be noted that although the vortex has lost a significant amount of its strength, the vortex shape is very well preserved after 45 radii of travel.

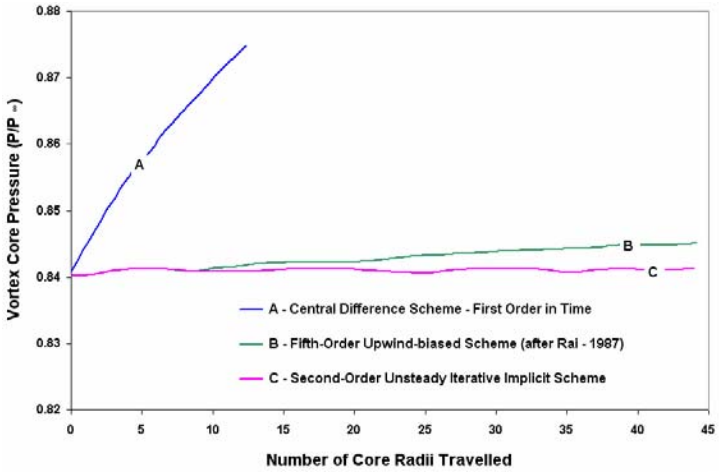

Figure 2: Vortex core pressure decay rate for three different schemes.

Figure 3: Pressure contours at Initialization (top) and after vortex has travelled 45 radii (bottom) 2nd-order iterative implicit scheme

2.3 SECOND-ORDER TIME ACCURATE ITERATIVE IMPLICIT SCHEME

The basic scheme used is a Linearized Block implicit ADI procedure of Briley and McDonald [21]. The splitting error and the linearization error associated with this basic scheme are removed by introducing an inner ADI iterative procedure at each time step. The temporal accuracy is increased to second-order by using three-point backward time differencing. On convergence of the inner iteration, the scheme becomes a fully implicit nonlinear backward time difference scheme. A more detailed discussion of these improvements is given by Rai [20] and such an iterative implicit three-time level ADI scheme is used in the present study. In addition, three point central differences are used to approximate the spatial derivatives. The spatial accuracy is second-order except for the use of numerical dissipation discussed subsequently.

When calculating high Reynolds number using either the Euler equations or the Navier-Stokes equations, using centred spatial differencing, some artificial dissipation is usually needed to maintain numerical stability and to suppress spurious oscillations in the numerical results. The approach used in the present effort is based upon the use of a second-order anisotropic artificial dissipation term. Introduction of the second-order terms for artificial dissipation formally reduces the scheme to first-order. However, the added second-order artificial dissipation term is preceded by an adjustable parameter which can be reduced so as to progressively reduce the effect of this term. The parameter, termed AVISC in the figures which will be presented, is essentially equivalent to a coordinate dependent inverse cell Reynolds number so that a specification of AVISC of 0.05 limits the maximum cell Reynolds number to 20. Obviously, artificial dissipation is a source of false diffusion and distortion of a vortex convected in a finite-difference grid. In the present work, the effects of artificial dissipation on the vortex structure are minimized by specifying a small value of the adjustable parameter which controls the amount of added dissipation, and this value is determined from a separate set of calculations in which the effects of this parameter's magnitude on the preservation of the free vortex convected over a long distance are examined. The values used for this parameter have some effect on the results, as will be demonstrated. In some cases a value of zero could be used but it was not determined that this was true in all cases. Consequently for safety a small valve of AVISC was used routinely. The variation of vortex core pressure with number of core radii is shown by curve C in Figure 2, which indicates a very stable and accurate solution. There was no significant distortion of the vortex during this travel. Contours of pressure at initialization and after 45 radii of the vortex travel are also shown in Figure 3.

2.4 EFFECTS OF SPATIAL SPACING ON THE SOLUTION ACCURACY

Two calculations were performed on grids with different spacing to study the effects of grid spacing on the vortex preservation. The first grid has the spacing of $\Delta x = \Delta y = ¼$, and the second grid is a finer grid with the spacing of $\Delta x = \Delta y = 1/8$. Variation of vortex core pressure versus number of core radii traveled for both grids is shown in Figure 4. It can be seen that numerical solution for the coarser grid is oscillating, particularly toward the latter parts of the vortex travel. Contour plots of pressure after 45 radii (not shown) showed a badly deformed vortex. Variation of vortex core pressure with number of core radii for the finer grid shown by the curve B in Figure 4, indicates a very stable and accurate solution. In contrast to the coarser mesh case, this case showed no significant distortion of the vortex during its travel.

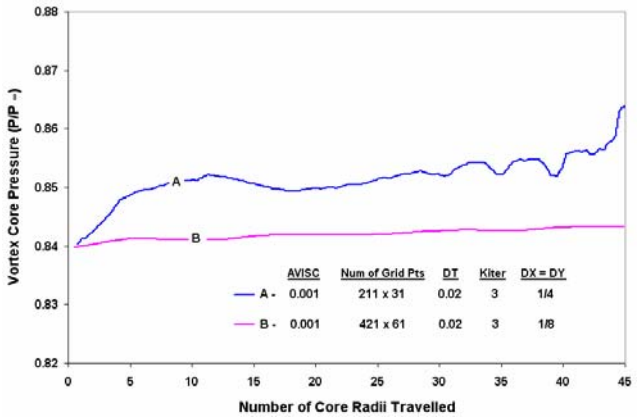

Figure 4: Effects of the grid spacing

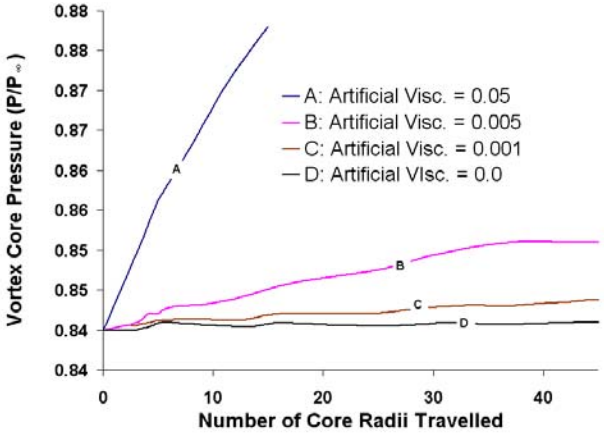

Figure 5: Effects of the Numerical Dissipation

2.5 EFFECTS OF NUMERICAL DIFFSUSION

Use of artificial diffusion enhances the stability and convergence properties of the numerical solution procedures. Such artificial diffusion could be added via the spatial differencing formulation (e.g. one-sided difference approximations for first derivatives) or by explicitly adding an additional diffusion term. In the numerical scheme used in this study the latter approach was adopted, since when an additional term is explicitly added, the physical approximation being made is usually clearer than when dissipative mechanisms are contained within numerical truncation errors, and further, explicit addition of an artificial viscosity term allows greater control over the amount of non-physical numerical dissipation being added. Obviously, the most desirable technique would add only enough numerical dissipation to suppress oscillations without deteriorating solution accuracy. Four cases, including zero artificial diffusion, were run to assess the effect of the numerical diffusion on the unsteady vortex flow and to help choose values which would preserve accuracy and yet suppress the oscillation. Variation of the vortex core pressure versus number of core radii travelled by the vortex for different values of the artificial viscosity is given in Figure 5. The parameter "AVISC" indicated in the figure is a measure of the amount of artificial viscosity added. The larger the AVISC value, the larger the added artificial viscosity. A value of 0.5 corresponds to a first order upwind difference level of numerical dissipation. The values used are 0.0, 0.001, 0.005, and 0.050. It is clear from these curves that the higher the value of the artificial viscosity the more dissipative the calculation. It should be noted that in the present calculation the solution remains stable without any added artificial viscosity throughout this calculation. Contours of pressure and vorticity magnitudes after 45 radii of travel for calculations with different values of artificial viscosity indicated that the vortex shape is very well preserved after 45 radii of travel, despite the fact that for higher values of artificial viscosity the vortex has lost more of its strength.

2.6 DIAGONAL CONVECTION

This case is conducted to evaluate the capability of the code in preserving the vortical structures travelling diagonal to the grid lines and in a direction not aligned with a coordinate direction. With the capability to convect a vortex in any direction, one could study the interaction of a vortex flowing into a blade in any arbitrary direction.

The computation was done using the second order accurate iterative implicit scheme. A lamb type vortex as described 2.0 is initialized in a bottom corner of a rectangular domain and is convected by the flow diagonally to the opposing corner. Contours of the static pressure at the initial condition are shown in Figure 6, with the inflow angle at a 45 degree angle to the x-coordinate direction. Contours of the pressure after the vortex has travelled 20 radii and 45 radii are also shown in this Figure. Grid size for this calculation was 337 x 337. It is noticed that the vortex has maintained its structure. Furthermore, monitoring the vortex core pressure along its path was similar to the curve C, shown in Figure 2, indicating that the vortex has preserved its strength in a diagonal to gird lines path, under this numerical scheme.

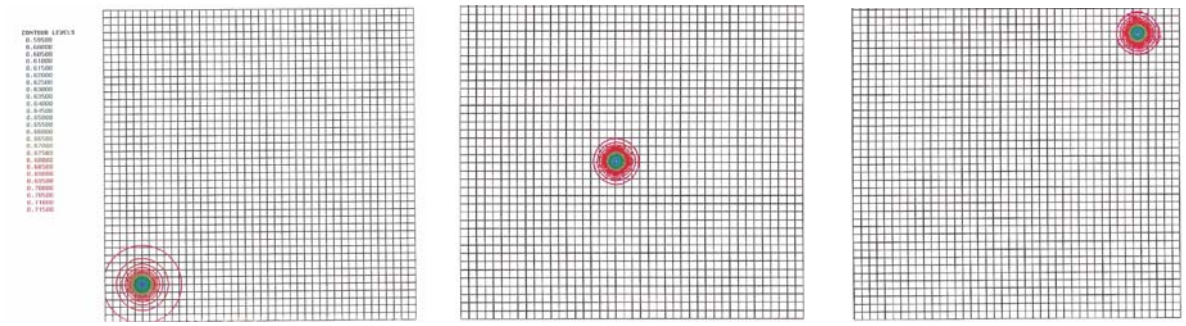

Figure 6: Pressure Contours for the Vortex in a Diagonal Convection. Dx = Dy = 1/8, every 8th grid line is shown.

3.0 BLADE VORTEX INTERACTIONS (BVI)

The interaction of concentrated vortices with blades induces unsteady aerodynamic loading responsible for blade vibrations, aeroelastic instabilities, and impulsive noise. The effects of blade-vortex interaction (BVI) are especially significant in the transonic flow regime, in which the strength and position of the shock waves are sensitive to small changes in the flow parameters. At the present time, a key problem in computing flows containing concentrated vortices is the ability to preserve and convect these vortices in a finite difference or finite-volume grid without false numerical diffusion due to truncation error, artificial dissipation and turbulence modelling. In this work, the ensemble-averaged, time-dependent Navier-Stokes equations are solved on a body-fitted grid around a NACAO012 airfoil to study strong interaction of a vortex with a stationary blade. The Navier-Stokes equations are solved by using an iterative implicit finite difference scheme with second order spatial and temporal accuracies. Furthermore, simple vortex preservation techniques discussed earlier are used to minimize the amount of spurious numerical dissipation and eddy viscosity caused by the presence of the vortex during its convective motion towards the leading edge of the blade. If a numerical procedure does not preserve an isolated vortex, this same procedure can not be used for the blade vortex interaction study since non-physical dissipation will occur prior to the interaction process and the process will be based upon a vortex of artificially low strength and large extent.

3.1 FLOW PARAMETERS

The reference length is the chord length of the blade and the reference flow conditions are the free stream condition with M_∞ = 0.8 and Re = 1.0 x 10^6. The background flow is a steady transonic flow with shock waves standing in the middle of the blade. Furthermore, the flow is symmetric about the chord line; hence, the lift coefficient (CL) is zero. The surface pressure distribution of this background flow is shown in Figure 7. The dimensionless strength and core radius of the vortex are -1.6 and 0.2, respectively, where the minus sign indicates that the vortex has a clockwise sense. The initial location of the vortex center is at a point 5 chords upstream of the airfoil leading edge (x_v = -5.0) and 0.26 chords below (Y_v = -0.26). The calculation is carried out from t = 0 to t = 8 with constant time step Δt = 0.005. It is noted here that the vortex core arrives at the blade leading edge when t = 4.95, which indicates an average core velocity of 0.99 v_∞.

The total number of grid points used is 144 x 118. The inflow boundary is located at 7 chords from the blade leading edge while the outflow boundary is located at 5 chords from the blade trailing edge. Based upon the isolated vortex study the distance between the top boundary and the chord line of the NACAO012 airfoil was set at 5 chord lengths. The geometric configuration is symmetric about the chord line. Along the inflow boundary, the total pressure, the total temperature and the inflow angle are specified. Along the outflow, top and bottom boundaries, the static pressure is specified; the velocity and the total temperature are obtained by extrapolation. On the blade surface, non-slip conditions are imposed. The density is obtained by solving the continuity equation and the surface temperature is specified as the constant, free stream total temperature.

3.2 BVI SIMULATION RESULTS

The interactions between the vortex and the blade with a shock are further elucidated in terms of the instantaneous static pressure distribution at several selected time stations. Figure 6 gives the pressure contours over the entire computational domain at t = 0. Distribution of static pressure coefficient on the blade surface at t = 0 is also shown in this Figure. This is the starting flow field. As the vortex convects towards the blade, the upper surface shock moves in the upstream direction, its strength is decreasing and the extent of the associated supersonic pocket also is reducing. On the other hand, the lower surface shock moves in the downstream direction with increased strength. In addition to the motion of the shock waves, pressure difference between the upper and lower surfaces start to build up. These generic features are illustrated in Figures 8 and 9. The upper surface supersonic pocket practically has disappeared. The lower surface shock wave becomes stronger and is located in a further downstream position; at the shock's root the flow shows signs of separation. The emission of a high pressure pulse from the upper surface of the leading edge is evident from Figure 9; this high pressure pulse then propagates upstream in a domain including the frontal region of the entire leading edge. Between this frontal high pressure region and the lower surface shock wave, a low pressure pulse is propagating towards the lower outer boundary. The general features of the flow at t = 6.0 are: the existence of a supersonic pocket on the lower surface, significant flow separation originating at the root of the shock, the appearance of vortex remnants near the blade trailing edge, and the development of supersonic flow on the upper surface. The flow on the lower surface does not exhibit any appreciable separation and is entirely transonic. Furthermore, about 70% of the upper surface is covered by a supersonic pocket, with compression waves appearing near the trailing edge of the blade. It is clear that the interaction is a strong one and the vortex path particularly, when the vortex is near the blade is influenced by the blade and the interaction. The local velocity changes significantly during the interaction. This makes techniques based upon assumed vortex position or shape unlikely to provide an accurate simulation.

This calculation clearly demonstrated the ability of the code in accurately convecting a vortex that was initially located far upstream of the blade, downstream toward the blade, and showed the flow development as the vortex interacted with the blade.

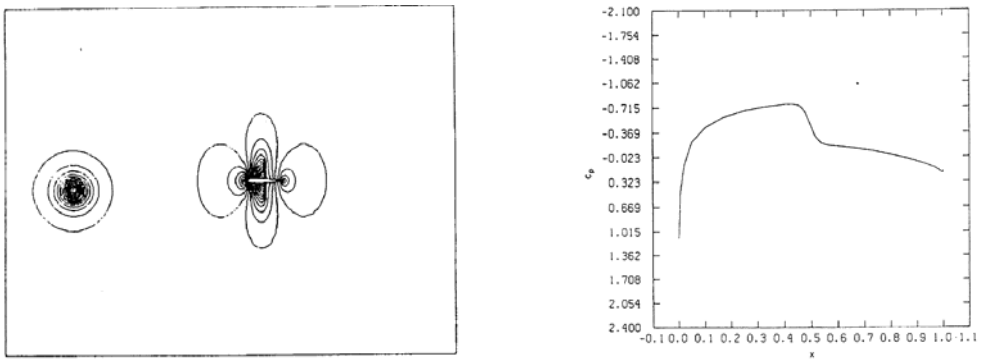

Figure 7: Static Pressure contours and the surface pressure coefficient C_p at t = 0.0

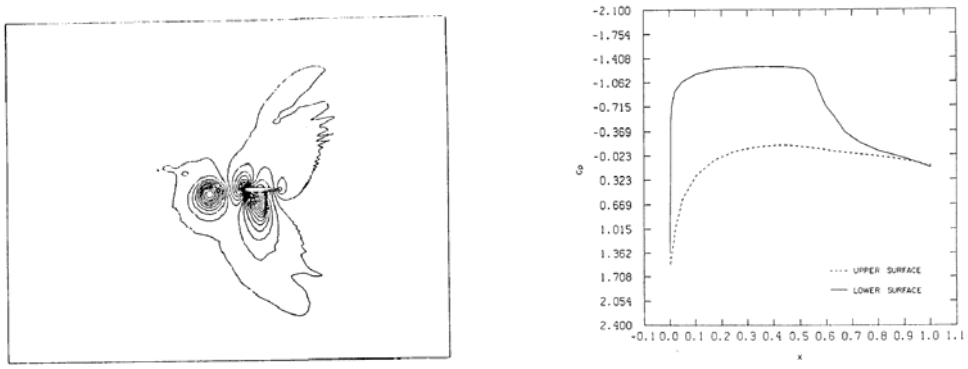

Figure 8: Static Pressure contours and the surface pressure coefficient C_p at t = 4.0

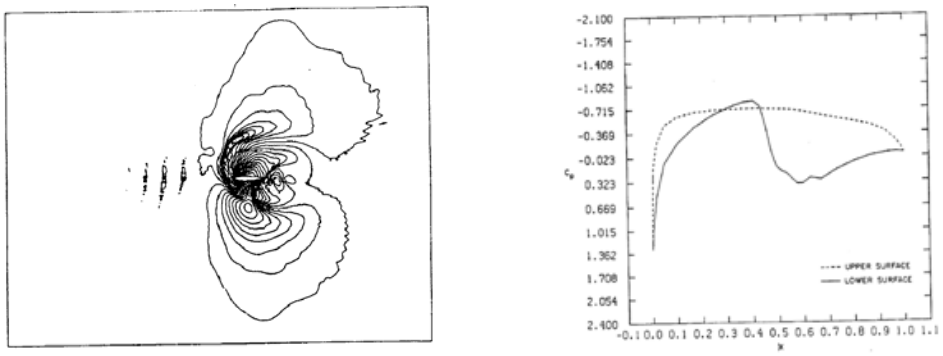

Figure 9: Static Pressure contours and the surface pressure coefficient C_p at t = 6.0

4.0 SUBMARINE MANEUVERS

The prediction of the maneuvering characteristics of underwater vehicles requires the accurate calculation of highly complex hydrodynamic phenomena which are not amenable to simple analytic techniques. Maneuvers of most bodies are difficult to predict due to large angles of attack and the presence of unsteady flow conditions. Underwater vehicles pose an added challenge because the control surfaces used for generating the necessary forces and moments during the maneuver are often relatively small compared to the overall size of

the buoyant body itself. Consequently, viscous forces and moments generated on the hull and appendages can have a dominant role in the behavior of the vehicle. Additionally, boundary layer and vortex wakes generated by the hull and forward appendages interact with the stern appendages, as well as with the propulsor, to provide forces and moments and vehicle dynamics significantly different from that which would be experienced without such interactions.

The propulsor is an important element in the overall maneuvering character of the vehicle, and it adds considerable further complexity to any predictive effort. Traditionally, an underwater vehicle propulsor is located at the stern to benefit from operating in the vehicle's wake. However, the wake region introduces a non-uniform inflow to the propulsor, and this often leads to out-of plane forces, in addition to the direct thrust and moment produced by the propulsor. These out-of-plane forces can produce significant moments, because the propulsor is often located a considerable distance from the center of gravity of the vehicle. The interaction of flows associated with the hull, appendages and propulsor produces a highly complicated unsteady hydrodynamic system.

One approach for prediction of the trajectory of submarines is to perform numerical simulations based on the Unsteady Reynolds-Averaged Navier-Stokes (UnRANS) equations. A physics-based prediction of the maneuvering characteristics can be obtained by coupling forces and moments data from these solutions with a six degree of freedom (6-DOF) rigid body motion analysis. Such computer simulations can provide both quantitative analysis and improved understanding of flow phenomena affecting both design and maneuverability. This information can contribute to both improved designs and the safe operation of submarines. Details of the numerical scheme and development of the method is given in detail in [22]. Here validation aspects of the method are described.

Flow around a maneuvering submarine with sailplanes, stern appendages, and a rotating propulsor include many vortical structures such as sail vortex, sailplane vortices, tip vortices emanating from stern appendages and propulsor blades, hull vortex feeding sheet, necklace vortices generated in the root of the sail, and in the root of the sailplanes. These vortices affect the forces and moments on the body of the vehicle and consequently the maneuvering characteristics of the vehicle. Preservation of these vortices by the code is therefore essential. A vortex preservation computation as described in 2.0 is conducted on the flow solver code. Based on that calculation appropriate turbulence model, grid density, dissipation factor, and time step were chosen to conduct the maneuvering computations [23].

4.1 VALIDATION STUDIES

Numerous solutions at several angles of drift were computed for a submarine configuration (named SUBOFF) with four stern appendages. Figure 10 shows contours of the x-component of vorticity for the 18° drift angle case. Flow traces are also drawn on the Figure 10. The x-vorticity contours together with the flow traces show the creation of two strong vortical structures emanating from the hull. The computed axial force and lateral force coefficients are also compared with the experimental data on the Figure 10. The computed force and moment coefficients are in extremely good agreement with the measured data (much better than anticipated at the time), even up to the maximum drift angle of 18 degrees. The effects of the capturing vortical structures are clearly indicated in the axial and in the lateral force coefficients. The Baldwin-Lomax turbulence model is used in these calculations.

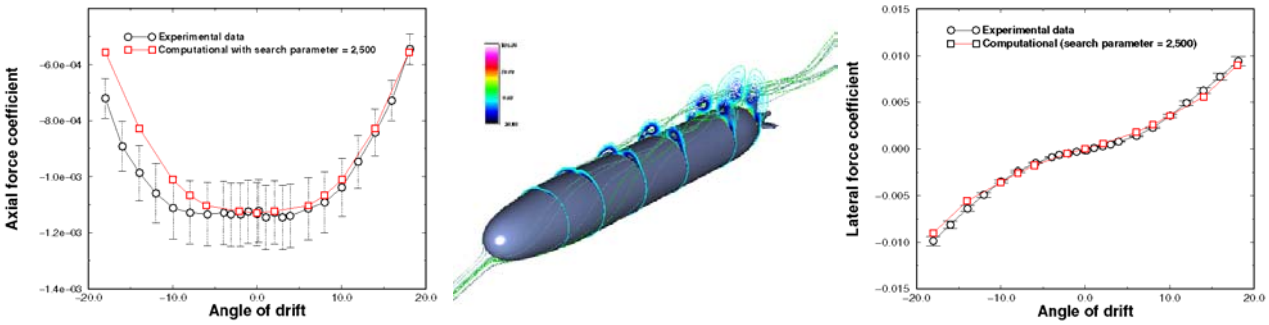

Figure 10: Contours of X-component of Vorticity - Experimental Data vs Computational

4.2 SIMULATION OF CRASHBACK MANEUVER

Deceleration of a self-propelled underwater vehicle by means of reversing the angular velocity of the propeller is called a crashback maneuver. This maneuver has been simulated [22] by computing a starting solution for a constant-speed vehicle and then decreasing the propeller rotation from the constant-rpm forward rotation speed, through zero to a constant-rpm reverse rotation. This calculation represents the most severe off-design condition for flow through the propeller and demonstrates capability to compute a very complex phenomenon regarding both the flow field and the vehicle dynamics. During this maneuver, the vehicle continues to move in a forward direction. Relative to the vehicle itself, the fluid generally flows towards the stern, with path-lines passing outboard from the propeller. The reversed rotation of the blades moves the fluid near the propeller in an upstream direction. These downstream and upstream fluid motions create a shear stress and, subsequently, generate a ring vortex located just outboard and downstream of the propeller blade tips. Figure 11 shows this vortex ring at some instant in time. Contours of the flow traces vary with the magnitude of the velocity, while the blades show contours representing the magnitude of the static pressure. The unsteady motion and eventual decay of this ring vortex generates unsteady side forces and has a pronounced effect on the behavior of the vehicle. The time history of propeller speed, vehicle velocity, forces, and circumferential position of the ring vortex relative to the blades are also shown in Figure 11. The lateral force Fy and the vertical force Fz display large-amplitude, large wavelength oscillations between positive and negative values. The oscillations are virtually identical for the two force components, except for the expected 90° phase difference. These out-of-plane forces also have small-amplitude high-frequency oscillations (associated with the blade-passing frequency) superimposed on these low-frequency oscillations. Figure 11 also shows a trace that represents the approximate circumferential position of the low—pressure region of the ring vortex (or rotating stall cell) at selected instants in time. In this trace, the circular symbols indicate the approximate circumferential position of this low-pressure region or cell, measured from the stern plane in the clockwise direction looking upstream. Each symbol is plotted as a sine of its angular position θ, and the dotted line is a least-squares polynomial fit.

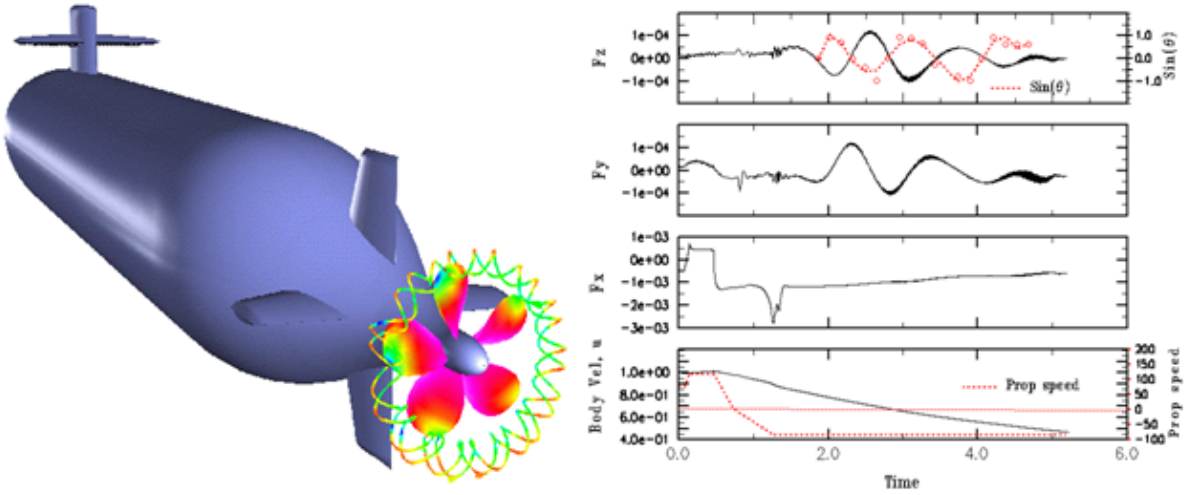

Figure 11: Vortex Ring Produced by the Crashback Maneuver (left) - Time History of Propeller Speed, Vehicle Velocity, Forces, and Circumferential Position of the Ring Vortex Relative to the Blades (right)

4.3 SIMULATION OF DEPTH-CHANGING MANEUVER

Most maneuvers other than crashback are accompanied by movement of one or more control surfaces. Control surface movement increases grid size and complexity, due to control surface gaps and movement. A simpler but approximate approach is to model the effect of control surface movement by imposing external forces to fixed control surfaces. This approach is demonstrated here for a simple depth-changing maneuver by externally changing the magnitude of the forces and moments on the horizontal stern planes, inducing a pitching moment about the center of gravity, and this leads to a rise or dive of the vehicle. Figure 12 shows the pressure distribution on the surface of the fully appended SUBOFF at an instant of time during the rising maneuver for which the pitch angle is about 23 degrees and the angle of attack is about 13 degrees. Since the vehicle is pitching about its center of gravity, which is located approximately half way between the bow and stern, the stagnation point on the nose moves toward the upper part of the nose, and the stagnation points on the tip of the horizontal stern planes move toward the lower surface of the planes. Once the vehicle has elevated to a certain level, the applied forces on the horizontal stern planes are decreased to reverse the direction of the moment from a pitch-up moment to a pitch-down moment. Figure 12 shows the pressure distribution later in time, after the vehicle motion has reversed from pitch-up to a pitch-down course. Comparing the location of the stagnation points on the nose of the hull and the tip of the horizontal stern planes at the pitch-up and pitch down maneuvers, it can be seen that the stagnation points have shifted to opposite sides. The time history of the vehicle inertial position and the applied z-direction force on the top surface of the stern plane are shown in Figure 12.

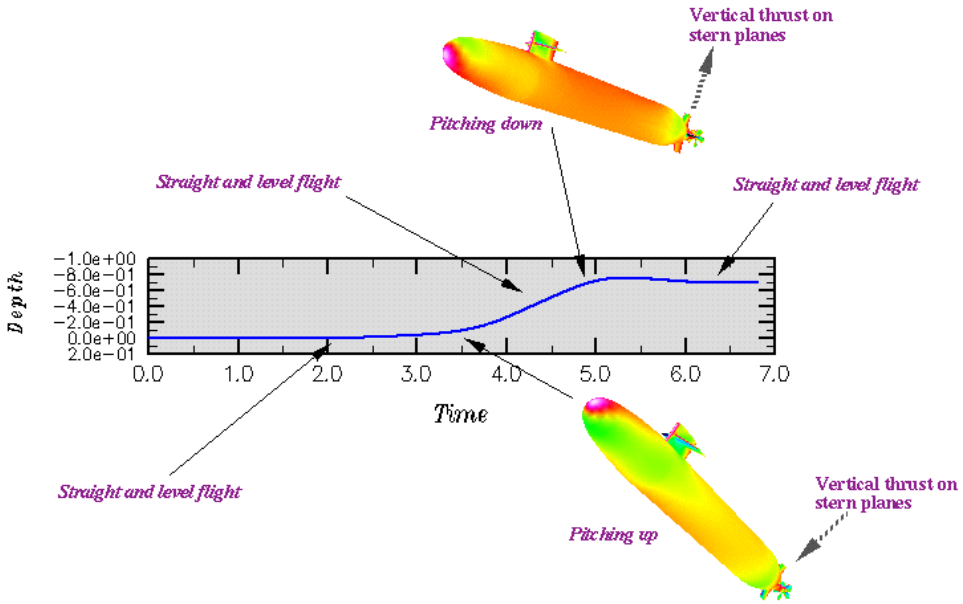

Figure 12: Surface Pressure Distributions and Trajectory prediction during a Depth-Changing Maneuver

5.0 SIMULATION OF A REACTING FLOW IN A GASEOUS TURBINE COMBUSTOR

Gas turbine combustors are designed to operate with stable flames. To produce a good mixing of the reactants and a stable flame, the reactants usually pass through some swirlers before entering the combustion chamber and the resultant flow in the chamber is a very high swirling flow. The simulation presented here demonstrates the capability of the code in generating and maintaining the vortical structures inside the combustion chamber. For validation, the computed results are compared with the experimental data.

5.1 EXPERIMENTAL SETUP AND THE GEOMETRY

The schematic of the experimental model gas turbine combustor operating on air/methane is shown in Figure 13. The experimental work is performed by Bowman. T.C. and Edwards, C. [24]. The operating condition of the gaseous combustor is also summarized in the Figure 13. The overall combustor assembly consists of three distinct sections: fuel delivery, main combustion chamber, and a tailpipe. Flow is delivered through two separate co-annular concentric pipes. The low velocity methane fuel is delivered through the inner pipe, whereas the higher velocity air is delivered through the annulus of the two pipes. Both fuel and airflows pass through 45° helical co-swirling swirlers and become highly swirling flows as they enter the main combustion chamber. This is necessary for creating a lifted, stable flame and for good mixing of the reactants. A close-up of the 45° helical co-swirling swirlers is also shown in Figure 13.

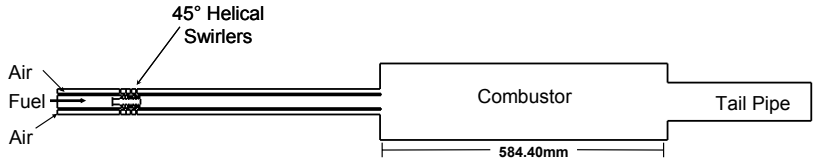

Equivalence ratio Φ = 0.67 ± 0.02	Mass flow rate g/s	Mean velocity m/s	Rey #
Air	30.7 ± 0.5	23	14000 (based on gap height)
Methane	1.20 ± 0.02	3.9	5800 (based on diameter)

Figure 13: Axial cross section and operating condition of the gaseous combustor operating on methane fuel

5.2 REACTING FLOW RESULTS

The numerical simulations performed to describe the flow, solve the Reynolds-Averaged Navier-Stokes equations on an unstructured discretization with added turbulence, chemical species, and combustion models. Turbulence is modelled by a cubic non-linear k-epsilon model with low Reynolds number wall integration [25]. The chemistry-turbulence interactions are represented by the eddy-dissipation combustion model of Magnussen and Hjertager [26], where combustion rate is assumed to be controlled by the turbulence mixing rate of the reactants.

The flow structures predicted by the numerical simulation are shown in Figure 14. It is dominated by a very strong center recirculation zone, and by another ring vortex generated in the upstream corner of the combustor. These clearly demonstrate the capability of the code in predicting these flow structures.

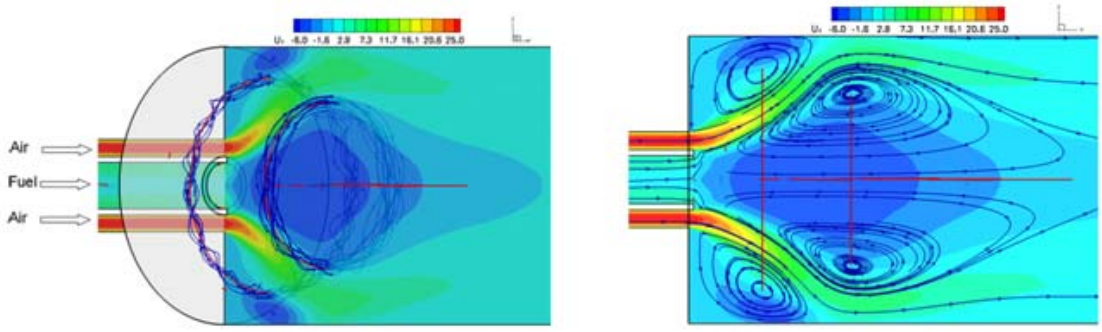

Figure 14: 3-D (left) & 2-D (right) Flow structures, showing Ring Vortices, Recirculation zones Axial Velocity, and particle traces (red dashed lines are vortex cores)

Figure 15, shows an axial cross section showing the computed axial velocity contours, azimuthal contours, axial, and azimuthal velocity profiles for both the computed and the measured data throughout the reacting field. The axial velocity is high in the air stream and the air jet quickly spreads toward the combustor wall. The central recirculation zone around the centerline with a length approximately equal to the diameter of the

combustor is maintained. Further, another recirculation is formed close to the wall. These recirculation zones are well captured by the simulation. Re-circulating hot gases in the center and the bulkhead corner section causes flame stabilization.

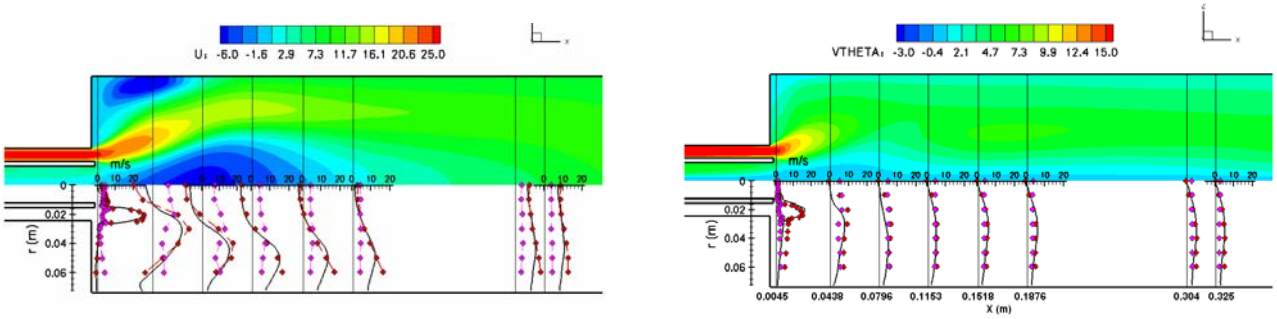

Figure 15: Axial & Azimuthal Velocity Contours & Radial Profiles
Red diamond symbols are the experimental data, solid lines are the computational data,
Pink diamond symbols are experimental velocity fluctuations about the mean
(They are used as the 50% confidence interval about the mean)

Good agreements between the computational results and the experimental data validate the suitability of the code for simulation of high swirl and reacting flows in combustion chambers.

6.0 SUMMARY AND CONCLUSION

Any computational code used for simulation and analysis of the flow in or around real-world devices and vehicles is required to predict the flow features and the flow quantities associated with these devices and vehicles with reasonable accuracy and in a reasonable time frame. The method of vortex preservation presented in this paper offers an approach where the time-accurate computational results are compared with the exact solution for a Lamb type vortex convecting in a free stream. Comparing the computed results with the exact solution eliminates the uncertainties that exist with the experimental data commonly used for the validation of the CFD codes. This method considers effects of the grid density, numerical dissipation, turbulence model, and grid alignment on the computed results. It is shown that if a numerical scheme can not preserve an isolated vortex, it can not be used for investigation of the flowfields that contain these flow structures.

Three real world scenarios, each with different flow characteristics are presented where the preservation of the vortical structures are critical to the outcome of the simulations. These included the blade vortex interaction (BVI) flow, flow around self-propelled maneuvering submarines, and the reacting flow in a gaseous combustor. The computed results were compared with the experimental data or the exact solution, when available. In many cases the original code proved to be incapable of preserving the flow features experienced in the real world. These codes were accordingly modified to include these capabilities. The final codes used for the simulations were developed to capture and maintain the flow structures associated with each case.

A new method was validated for predicting trajectory of appended underwater vehicles with rotating propulsors. The validation work included trajectory predictions for a fully-appended submarine going through a crashback maneuver and a depth-changing maneuver. Furthermore, the results of a number of computations performed on a SUBOFF geometry with four stern appendages were compared with experimental data. The comparisons showed excellent agreements.

An experimental model gas turbine combustor exhibiting the typical flow features associated with gas turbine combustors was numerically modelled to demonstrate the modelling capabilities of another computer code in predicting the flow characteristics of these combustors. The computed results were validated against the experimental data. Flow features specific to gaseous combustion chambers such as recirculation zones were also captured by the simulations.

7.0 REFERENCES

[1] Roach, P.J., *"Qualification of Uncertainty in Computational Fluid Dynamics,"* Annual Review of Fluid Mechanics, Vol. 29, 1997, pp. 123-160.

[2] Roach, P.J., *"Verification and Validation in Computational Science and Engineering,"* New Mexico, USA, Hermosa Publishers. http://www.hermosa-pub.com/hermosa

[3] Aeschliman, D.P., W.L. Oberkampf, and F.G. Blottner, *"A Proposed Methodology for Computational Fluid Dynamics Code Verification, Calibration, and Validation,"* Paper presented at the 16th International Congress on Instrumentation in Aerospace Simulation Facilities (ICIASF), July 18-21, 1995, Wright-Patterson AFB, OH 45433.

[4] Aeschliman, D.P. and W.L. Oberkampf, *"Experimental Methodology for Computational Fluid Dynamics Code Validation,"* AIAA Journal, Vol. 36, No. 5, pp. 733-741.

[5] Barber, T.J., *"Role of Code Validation and Certification in the Design Environment,"* AIAA Journal, Vol. 36, No. 5, pp. 752-758.

[6] Bardina, J.E., P.G. Huang, and T.J. Coakley, *"Turbulence Modeling Validation, Testing, and Development,"* NASA TM 110446, April 1997.

[7] Benek, J.A., E.M. Kraft, and R.F. Lauer, *"Validation Issues for Engine - Airframe Integration,"* AIAA Journal, Vol. 36, No. 5, pp. 759-764.

[8] Blottner, F.G., *"Accurate Navier-Stokes Results for the Hypersonic Flow over a Spherical Nosetip,"* AIAA Journal of Spacecraft and Rockets, Vol. 27, No. 2, pp. 113-122.

[9] Bobbitt, P.J., *"The Pros and Cons of Code Validation,"* AIAA Paper 88-2535 (NASA TM 100657), July 1988.

[10] Coleman, H.W. and F. Stern, *"Uncertainties and CFD Validation,"* ASME Journal of Fluids Engineering, Vol. 119, December 1997, pp. 795-803.

[11] Cosner, R.R., *"Issues in Aerospace Application of CFD Analysis,"* AIAA Paper 94-0464, January 1994.

[12] Cosner, R.R., *"CFD Validation Requirements for Technology Transition,"* AIAA Paper 95-2227, June 1995.

[13] Roache, P.J., K. Ghia, and F. White, "*Editorial Policy Statement on the Control of Numerical Accuracy,*" ASME Journal of Fluids Engineering, Vol. 108,No. 1., March 1986, p. 2.

[14] AIAA, *"Editorial Policy Statement on Numerical Accuracy and Experimental Uncertainty,"* AIAA Journal, Vol. 32, January 1994, p. 3.

[15] AIAA, "*Guide for the Verification and Validation of Computational Fluid Dynamics Simulations,"* AIAA G-077-1998, 1998.

[16] ASME Editorial Board, *"Journal of Heat Transfer Editorial Policy Statement on Numerical Accuracy,"* ASME Journal of Heat Transfer, Vol. 116, November 1994. pp. 797-798.

[17] H. Lamb, "*Hydrodynamics,"* 6th edn. Cambridge (1957).

[18] S. -N. Liu, F. Davoudzadeh, W. R. Briley, and S. J. Shamroth: "*Two- and Three-Dimensional Blade Vortex Interactions*", NASA Contractor Report 177567, prepared for NASA Ames Research Center, 1990.

[19] F. Davoudzadeh, S. -N. Liu, W. R. Briley, and S. J. Shamroth: "*Navier-Stokes Simulation of Transonic Blade-Vortex Interactions,"* ASME Journal of Fluids Engineering, Vol. 112, No. 4, pp. 501-509, 1990.

[20] M. M. Rai, "*Navier-Stokes simulations of blade-vortex interactions using high order accurate upwind schemes,"* .AIAA Paper 87-0543, 25th Aerospace Sciences Meeting, Reno, Nevada, 12-15 January (1987).

[21] W. R. Briley and H. McDonald, "*Solution of the multidimensional compressible Navier-Stokes equations by a generalized implicit method,"* J. Comput. Phys. 24, 372 (1977).

[22] F. Davoudzadeh, L. K. Taylor, W. C. Zierke, J. J. Dreyer, H. McDonald, and D. L. Whitfield: *"Coupled Navier-Stokes and Equations of Motion Simulation of Submarine Maneuvers, Including Crashback",* ASME Fluids Engineering Division Summer Meeting, Vancouver, Canada 1997.

[23] W. C. Zierke (ed.), F. Davoudzadeh (co-author): "*A Physics-based Means of Computing the Flow around a Maneuvering Underwater Vehicle",* Applied Research Laboratory Technical Report No. T 97-002, January 1997.

[24] Bowman, C.T., et al, 2002, "*Active Control of Combustion Instability in Air-Breathing Propulsion Systems – A Computational and Experimental Program*," Department of Mechanical Engineering, Stanford University, Final Technical Report, NASA-Glenn Grant No. NAG 2-1219.

[25] Shih, T.-H., Chen, K.-H., and Liu, N.-NS., 1998, "*A Non-Linear K-epsilon Model for Turbulent Shear Flows,"* AIAA Paper 98-3983.

[26] Magnussen, B.F., and Hjertager, B. H., 1977, "O*n Mathematical Modeling of Turbulent Combustion with Special Emphasis on Soot Formation and Combustion,"* Sixteenth Symposium (International) on Combustion, The Combustion Institute, pp. 719-729